

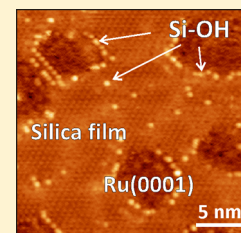
# Hydroxylation of Metal-Supported Sheet-Like Silica Films

B. Yang, E. Emmez, W. E. Kaden, X. Yu, J. A. Boscoboinik, M. Sterrer, S. Shaikhutdinov,\* and H.-J. Freund

Abteilung Chemische Physik, Fritz-Haber-Institut der Max-Planck-Gesellschaft, Faradayweg 4-6, Berlin 14195

## S Supporting Information

**ABSTRACT:** Adsorption of water on a metal-supported sheet-like silica film was studied by infrared reflection absorption spectroscopy (IRAS) and temperature-programmed desorption (TPD). As expected, the silica surface is essentially hydrophobic. Hydroxo species, primarily in the form of isolated silanols (Si–OH), were observed only upon water condensation at low temperatures and subsequent heating above 200 K. The amounts of silanol species account for less than a few percent of the surface Si atoms, and they are found to be thermally stable up to 900 K. Isotopic experiments showed that hydroxyls form almost exclusively from the adsorbed water molecules and do not undergo scrambling with the lattice oxygen atoms upon heating. Steps within the silica sheet, due to a terraced topography and/or the presence of “holes”, are proposed as the active sites for hydroxylation. The acidic properties of silanol species were studied with CO and NH<sub>3</sub> as probe molecules. In the case of ammonia, an H–D exchange reaction was observed between OD species and NH<sub>3</sub>, and the same reaction was found to occur for OD(OH) and H<sub>2</sub>O(D<sub>2</sub>O), respectively. The results are compared with those reported in the literature for amorphous silica.



## 1. INTRODUCTION

Silicon dioxide (SiO<sub>2</sub>) is a widely studied substance due to its importance in geology, materials science, microelectronics, and catalysis. The interaction of the silica surface with water plays an important role in natural processes such as weathering and dissolution. Also, it is generally accepted that the performance of silica in catalysis, where it may be involved as either the support or the active surface, is primarily determined by surface hydroxyl species.

Numerous, both experimental and theoretical, studies have been performed to better understand how water interacts with amorphous silica and quartz (see, for example, ref 1 and references therein). Analytical tools and spectroscopic techniques, including nuclear magnetic resonance, infrared (IR), and Raman spectroscopies, have been utilized to investigate hydroxy species on silica. Results from such work suggest the presence of both isolated silanols (i.e., single silanols, Si–OH, and geminal silanols, Si–(OH)<sub>2</sub>) and hydrogen-bonded silanols, which may, in principle, be differentiated by IR spectroscopy.<sup>1b,e,2</sup> Water molecules do not seem to adsorb on the regular, essentially hydrophobic siloxane (Si–O–Si) terminated surface, and this is in line with theoretical considerations for the reconstructed  $\alpha$ -quartz(0001) surface.<sup>1h,3</sup> Instead, it is generally accepted, primarily on the basis of IR studies, that water chemisorbs on silica by opening strained siloxane (Si–O–Si) bonds and thus forming two silanol groups.<sup>1e</sup> Subsequent water then adsorbs on the silanol-covered surface rather than the pristine siloxane surface.<sup>3</sup> Among the chemical strategies that have been used to characterize silica is H–D exchange via reaction with deuterated water, which has been employed, for example, to distinguish hydroxyl groups on the surface from those buried in the bulk of silica gel particles.<sup>4</sup>

Because of the structural complexity and diversity of silica, chemical properties of hydroxylated silica surfaces remain the

subject of many research studies. Application of surface-sensitive experimental techniques to silica-based materials, however, faces many technical difficulties, as these materials exhibit poor electrical and thermal conductivity. These issues may, in principle, be overcome through the use of thin silica films supported on metal substrates, which do not charge upon electron impact or emission and efficiently cool down to liquid nitrogen temperatures typical of such studies. Over the past decade, such samples have been extensively studied as suitable model systems of silica.<sup>5</sup> Via this approach, well-ordered silica structures have been prepared in the form of a “monolayer” film with SiO<sub>2.5</sub> compositional stoichiometry,<sup>6</sup> or a SiO<sub>2</sub> bilayer,<sup>7</sup> with both consisting of a two-dimensional, honeycomb-like network of corner-sharing [SiO<sub>4</sub>] tetrahedra. Thicker films behave virtually identical to amorphous silica overlayers thermally grown on Si surfaces.

Previous adsorption studies conducted over monolayer SiO<sub>2.5</sub> films on Mo(112)<sup>8</sup> showed that water almost exclusively binds via weak, nondissociative interaction with the surface. This, however, might be influenced by the strength of the Si–O–Mo linkages present in that case. By contrast, the ruthenium-supported bilayer film is only weakly bound to the metal substrate and, as such, resembles sheet-like silicates, albeit only one unit-cell thick versions thereof (see inset in Figure 1). Additionally, the bilayer films exhibit more structural flexibility than the monolayer versions and may exist in crystalline or vitreous forms, or both coexisting.<sup>9</sup>

In this work, we present the results of a study aimed at investigating water adsorption on bilayer silica films under vacuum conditions using infrared reflection–absorption spectroscopy (IRAS) and temperature-programmed desorption

Received: February 25, 2013

Revised: March 27, 2013

Published: March 27, 2013

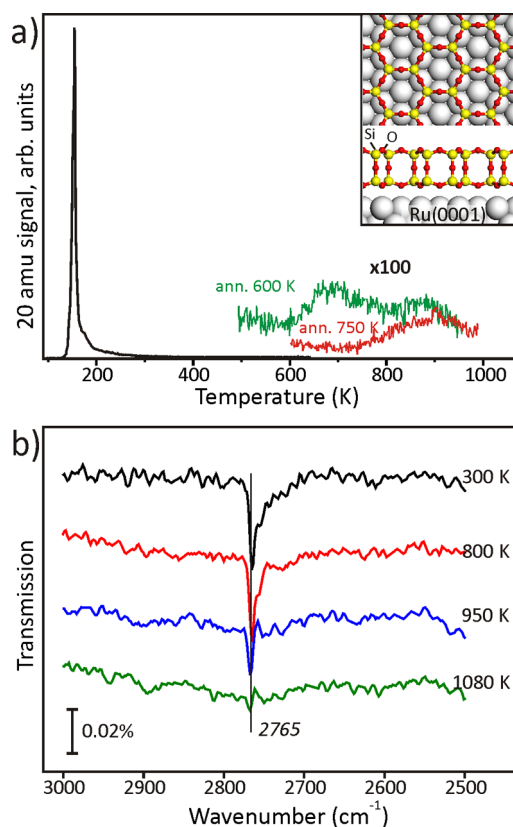


**Figure 1.** (a) TPD spectra (20 amu) of 5 L of  $D_2O$  adsorbed onto a bilayer silica film at 100 K and subsequently heated at a rate of 3 K/s. The green curve shows a typical spectrum for a sample preheated to 600 K to diminish the shadowing effect of the tail from multilayer water desorption. The red curve shows the spectrum of a sample preheated to 750 K. Both spectra reveal a desorption feature centered at 900 K. (b) IRA spectra of a film exposed to  $D_2O$  at 100 K and heated to the indicated temperature. The spectra were taken at 100 K and are offset for clarity. The inset in (a) depicts the atomic structure of the bilayer film grown on Ru(0001).

(TPD). In particular, we focus on the acidic properties of hydroxyl species via the adsorption of CO and  $NH_3$  probe molecules. The results are compared to those reported in the literature for bulky silica materials.

## 2. EXPERIMENTAL SECTION

The experiments were carried out in three ultrahigh vacuum (UHV) chambers (base pressure  $\sim 5 \times 10^{-10}$  mbar). One chamber is equipped with low-energy electron diffraction (LEED, from Omicron), an IRA spectrometer (Bruker IFS 66v), X-ray photoelectron spectroscopy (Scienta SES 200 hemispherical analyzer), and a scanning tunneling microscope (STM) (from Omicron). The Ru(0001) crystal (99.99% from MaTeck GmbH) was mounted on an Omicron sample holder, with the temperature measured by a Type K thermocouple spot-welded to the edge of the sample. Additionally, a pyrometer viewing the sample through a window at a fixed position was also employed to verify the accuracy of measurements made at elevated temperatures.

The second UHV chamber is equipped with LEED, Auger electron spectroscopy (both from Omicron), IRAS (Bruker IFS 66v), and a differentially pumped quadrupole mass spectrometer (QMS, from Hiden) for TPD measurements. In this setup, the temperature was measured by a Type K thermocouple spot-

welded to the back side of the crystal, which was, in turn, spot-welded to a pair of parallel Ta wires used for resistive heating to  $\sim 1300$  K and liquid nitrogen cooling to  $\sim 100$  K.

The final chamber houses equipment for low-energy helium ion scattering spectroscopy (ISS), LEED, XPS (all from Specs), and a differentially pumped QMS (Pfeiffer). Here, the sample was mounted in the same manner as that described for the first setup, with an e-beam heater employed to achieve higher heating rates and temperatures than those possible in the second setup.

In each case, the clean Ru(0001) surface was obtained following several  $Ar^+$ -sputtering and 1400 K UHV annealing cycles. Once clean, a  $3O(2 \times 2)$  overlayer was prepared by heating the clean surface to 1200 K for 5 min in  $3 \times 10^{-6}$  mbar  $O_2$ . After this, the sample was cooled, with oxygen pumped out at  $\sim 500$  K, and silicon (99.99%) then deposited onto the surface at  $\sim 100$  K in  $2 \times 10^{-7}$  mbar  $O_2$  using an e-beam assisted evaporator (EMT3, Omicron). To complete the preparation, final oxidation of the film was performed in  $3 \times 10^{-6}$  mbar  $O_2$  at  $\sim 1200$  K. Adsorption of CO,  $NH_3$ ,  $H_2O$ , and  $D_2O$  was performed using a directional gas doser (local pressure at the sample below  $10^{-6}$  mbar), and the IRA spectra were recorded using p-polarized light at an  $84^\circ$  grazing angle of incidence (spectral resolution  $4 \text{ cm}^{-1}$ ).

## 3. RESULTS AND DISCUSSION

**3.1. Water Adsorption on Ultrathin Silica Films.** Prior to water adsorption, the “as-prepared” films were characterized by IRAS, which revealed only two sharp and intense bands at 1300 and  $692 \text{ cm}^{-1}$ . Such features are characteristic of the well-established bilayer structure, which has been discussed in detail elsewhere.<sup>7</sup> LEED showed a  $(2 \times 2)$ -Ru(0001) pattern in conjunction with a  $(2 \times 2)$  diffraction ring, indicating the coexistence of both crystalline and vitreous silica domains in the films.<sup>9a</sup> On the basis of CO adsorption studies and previous TPD/STM results,<sup>9a</sup> we estimate that the presence of “holes” results in the exposure of  $<5\%$  of the underlying O-covered Ru(0001) support.

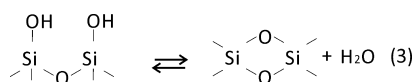
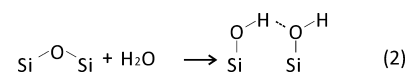
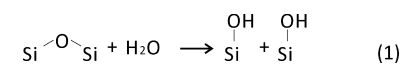
Adsorption of water onto the silica films at 300 K did not result in any IRAS detectable hydroxo species. (We primarily used deuterated water ( $D_2O$ ) to discriminate against reactions with residual water in the vacuum background.) This finding can be readily explained by the atomic structure of the silica bilayer film, which is terminated by an O-layer on either side and is, therefore, hydrophobic. To increase the sticking coefficient, water adsorption was performed at low temperatures ( $\sim 100$  K), resulting in an “amorphous solid water” film (or ice, for simplicity). This ice overlayer sublimates at  $T \approx 160$  K (Figure 1a) following zero-order kinetics (additional spectra are not shown here), upon which hydroxo species become clearly visible by IRAS (Figure 1b). Note that no OD species were found after the same treatment over the  $3O(2 \times 2)$ -Ru(0001) surface during control experiments.

The top spectrum in Figure 1b, which was obtained after heating to 300 K, shows a sharp signal centered at  $2765 \text{ cm}^{-1}$ . This peak can be straightforwardly assigned to  $\nu(O-D)$  stretching vibrations and readily shifts to  $3750 \text{ cm}^{-1}$  via D-H exchange upon exposure to  $H_2O$  at low temperatures (see Figure S1, Supporting Information). (Please keep in mind that it is common in IRAS to plot experimental spectra as the energy-dependent reflectance relative to that from a reference sample and that, in this case, data were collected from the same sample prior to water adsorption. Therefore, negative signals

indicate the appearance of new species, whereas positive signals show the disappearance of pre-existing ones.) In addition, we also note the presence of a prominent shoulder on the low frequency side of the main peak, which extends to  $2700\text{ cm}^{-1}$ . Accordingly,<sup>2b,c,10</sup> this can be attributed to hydrogen-bonded OD species but should be considered an upper limit for the nearest-neighbor hydroxyl concentration due to possible contributions from small amounts of water readsorption prior to performing our measurements at 100 K. Upon heating to elevated temperatures, the shoulder disappears, and the main peak gradually attenuates (Figure 1b). Apparently, D-bonded species desorb first, presumably due to a higher probability for the recombination of adjacent hydroxyls. The remaining isolated silanols fully desorb at  $\sim 1100\text{ K}$ , indicating their high thermal stability. Note, however, that powdered silica samples typically require temperatures well above 1200 K for full dehydroxylation,<sup>11</sup> most likely due to the diffusion limitations in these materials.

Consistent with the IRAS data, the TPD results also show recombinative desorption of hydroxyls in the form of water at high temperatures. Note that a long desorption tail extending to high temperatures is usually observed in TPD spectra of ice films and is commonly attributed to the low pumping rate of water. To diminish this effect, the sample was preheated to 600 K in the first TPD run and to 750 K in the second adsorption–desorption run, as shown in Figure 1a. Both desorption curves show a feature beginning at  $\sim 800\text{ K}$ , which is roughly consistent with the onset for disappearance of the principal IRA signal at  $2765\text{ cm}^{-1}$  (Figure 1b). On the basis of changes in the relative intensity of the lower temperature feature with variation in the duration of  $\sim 300\text{ K}$  annealing and the subsequent TPD heating rates, we have concluded that only the higher temperature feature relates to water evolution from the surface (i.e., lower temperature desorption in the range below  $T \approx 800\text{ K}$  arises from background sources unrelated to surface chemistry). From the integral intensity of the TPD signal observed for recombinative water from various samples, we estimate an upper limit of  $\sim 0.1\text{ nm}^{-2}$  for the surface density of silanols, which is roughly equivalent to one OH per every 40 six-membered rings (assuming the film is a perfectly ordered honeycomb-like structure). Therefore, we conclude that hydroxylation of the silica films occurs primarily on defects rather than regular sites.

It is generally accepted in the literature that hydroxylation of silica and silicalites proceeds via “opening” of asymmetrically strained siloxane bridge sites<sup>11b</sup> or edge-shared tetrahedral dimers,<sup>1e</sup> as shown schematically below:



This conclusion is based primarily on the inverse relationship between the intensities of bands in the  $890\text{--}910\text{ cm}^{-1}$  region (assigned to strained siloxanes)<sup>1e,11b</sup> and the  $\nu(\text{OH})$  band at  $3748\text{ cm}^{-1}$ .<sup>1e,h,10,11</sup> The vast majority of the studies on this subject have been carried out on high surface area silica samples prepared by “wet chemistry”, for which it has been generally concluded that strained siloxanes are formed by the recombination of surface silanols at elevated temperatures

following route 3. Contrastingly, IRAS studies of thin silica films by Chiang et al.<sup>12</sup> showed that such defects can be formed even on dry silica upon annealing to 1400 K. (In this case, the films were prepared by decomposition of a native silica film on a Si wafer, which was positioned in front of a polycrystalline Mo block in vacuo). The results of the latter study also indicated that the chemistry of silica is largely determined by the local structure rather than the global surface area.

Close inspection of the  $800\text{--}900\text{ cm}^{-1}$  region in our IRAS experiments did not reveal any features correlated with the degree of hydroxylation. Certainly, this can be due to the low detection efficiency of these bands, which are difficult to detect even on the powdered systems.<sup>12</sup> Nonetheless, following either mechanism 1 or 2, one of the two hydroxyl species should include a silica lattice oxygen atom and the other an oxygen atom from a dissociated water molecule. Therefore, one could, in principle, study the reaction mechanism and verify the proposed scenario by isotopic labeling of the oxygen in silica and water. Morrow et al.<sup>10</sup> have previously reported isotopic experiments with  $\text{H}_2^{18}\text{O}$ , but the samples studied already contained considerable amounts of residual  $^{16}\text{OH}$  species prior to the  $\text{H}_2^{18}\text{O}$  adsorption. Nonetheless, the results were used to justify the secondary reaction 2, which was thought to occur on sites other than those involved in reaction 1. Later, the presence of two types of defects (silanol-free and silanol-containing edge-shared defects) was suggested by Bunker et al.,<sup>1e</sup> with the silanol-free defect being much more reactive. To shed light on the hydroxylation mechanism for our films, we have performed isotopic experiments which can be easily carried out on the model system introduced here under well-controlled conditions.

Figure 2a displays a typical phonon spectrum from a silica film prepared with  $^{18}\text{O}$ , where the main bands are shifted by

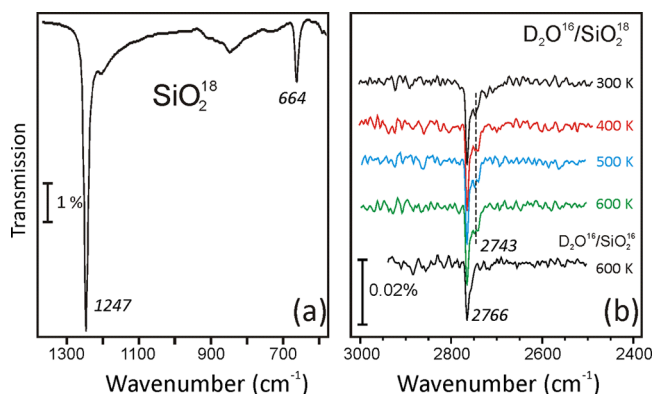


**Figure 2.** (a) IRA spectrum of a silica bilayer film prepared with  $^{18}\text{O}$ . (b) IRA spectra of the  $\nu(\text{OD})$  region following adsorption of  $\text{D}_2^{16}\text{O}$  on this film and heating to the indicated temperature. The spectra are offset for clarity.

predictable amounts to lower frequencies ( $1247$  and  $644\text{ cm}^{-1}$ , respectively) when compared to  $\text{Si}^{16}\text{O}_2$ . Following creation of this film, the surface was hydroxylated with  $\text{D}_2^{16}\text{O}$ , and the IRA spectra shown in Figure 2b were taken. Surprisingly, the initial (300 K) IRA spectrum of the  $\text{Si}^{18}\text{O}_2$  film, treated with  $\text{D}_2^{16}\text{O}$  at 100 K and heated to 300 K, is virtually identical to the hydroxylated film prepared with  $^{16}\text{O}$  (compare Figures 1b and 2b). Meanwhile, the signal from  $^{18}\text{OD}$  species, expected at around  $2750\text{ cm}^{-1}$  on the basis of the reduced mass analysis, is hardly discernible from the hydrogen-bonded  $^{16}\text{OD}$  shoulder noted

for the unlabeled film. As we heat the film to 600 K, however, we can begin to unambiguously note the presence of some  $^{18}\text{OD}$ , albeit with far less signal intensity than that for the  $^{16}\text{OD}$  feature.

In principle, these findings may have different explanations: (i) the hydroxylation of ultrathin silica films proceeds by way of a mechanism other than that commonly considered for three-dimensional amorphous silica and silicalites; (ii) the  $^{18}\text{O}-\text{D}$  bond is almost parallel to the surface and, as such, becomes nearly invisible in IRAS due to the so-called “surface selection rule,” which states that only vibrational modes that give rise to an oscillating dipole normal to the metallic surface are active;<sup>13</sup> (iii) the hydroxylation results in geminal silanols, i.e., with  $^{18}\text{OD}$  and  $^{16}\text{OD}$  attached to the same Si atoms, and the low-frequency band associated with  $^{18}\text{OD}$  is suppressed due to the so-called “intensity borrowing,”<sup>13</sup> where a higher frequency signal dominates the spectrum of a system consisting of strongly coupled oscillators;<sup>14</sup> and (iv) any combination of (i)–(iii). Note also that if the hydroxylation occurs on adventitious silica clusters and particles rather than on the silica film, then one would expect equal intensities of the two OD bands due to the random orientation of surface species on these particles with respect to the film normal.

To complement the experiments shown in Figure 2, we have also conducted isotope-exchange recombinative water TPD studies from  $\text{Si}^{18}\text{O}_2$  samples following low-temperature exposure to  $\text{D}_2^{16}\text{O}$  and subsequent annealing above room temperature. From the results, which are plotted in Figure 3a,

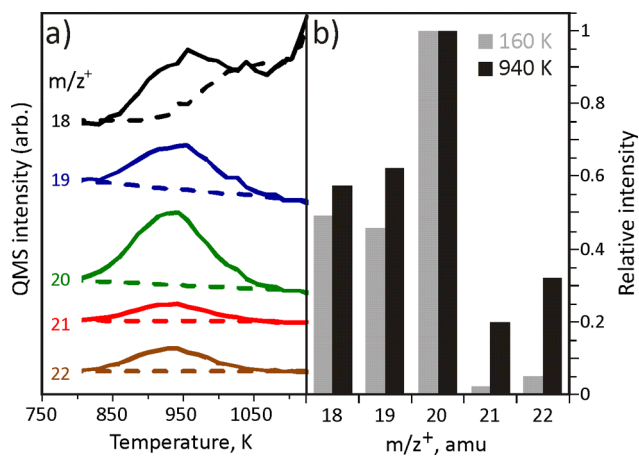


**Figure 3.** (a) TPD spectra (the heating rate 10 K/s) are shown as a function of constituent mass for the recombinative desorption of water from bilayer  $\text{Si}^{18}\text{O}_2/\text{Ru}(0001)$  following exposure to 5 L of  $\text{D}_2^{16}\text{O}$  at  $\sim 130$  K and subsequent heating to 300 K. The dashed lines indicate the backgrounds used for peak integration and are linear in all cases except  $m/z^+ = 18$ , where the background has been obtained by appropriately scaling the  $m/z^+ = 36$  desorption profile to account for  $^{18}\text{O}_2$  cracking contributions during the onset of  $^{18}\text{O}/\text{Ru}$  recombinative desorption. (b) The relative intensity of the time-integrated TPD signals for various mass channels during the desorption of multilayer ( $T_{\text{peak}} \approx 160$  K) and recombinative ( $T_{\text{peak}} \approx 940$  K) water are compared using the experimental data from (a).

we note detection of mostly  $m/z^+ = 18, 19,$  and  $20$  upon recombinative desorption of the dissociated water species. This is reflected in Figure 3b, which plots the relative intensity of the time-dependent peak integrals for each of the mass channels collected in Figure 3a during both multilayer ( $T_{\text{desorb}} \approx 160$  K) and recombinative ( $T_{\text{desorb}} \approx 940$  K) water desorption.

A careful analysis of this data, similar to that provided for ammonia desorption (see below and Figures S1 and S2 in Supporting Information), shows that the lower mass-channel domination of the distributions reflects desorption of predominantly  $^{16}\text{O}$  species. The large relative intensities for  $m/z^+ = 18$  and  $19$  reflect a significant concentration of H impurities within the  $\text{D}_2\text{O}$  dose, but this manifests itself to a similar degree in both desorption features. On the other hand, the significant abundance of  $m/z^+ = 21$  and  $22$  detected in the high-temperature feature is mostly absent during multilayer desorption and implies some degree of surface scrambling, such that  $\sim 25\%$  of the recombinatively desorbing water incorporates an  $^{18}\text{O}$  from the surface prior to departing. This is roughly consistent with the relative abundance of  $^{18}\text{OD}$  noted at lower temperatures via IRAS (Figure 2b) and is far less than would be expected if the desorption process proceeded by the recombination of freely diffusing D species meeting over randomly positioned O atoms. This latter finding indicates that desorption of water seems to occur nearly exclusively from the defect sites where the dissociative binding of the hydroxyls occurred, which provides more evidence that these sites are likely different in nature from those in the majority of the film.

One type of defect commonly considered in studies of epitaxially grown, thin-film oxides is domain boundaries. To this end, previous high-resolution STM studies of silica bilayer films showed that the crystalline phase smoothly transforms into the vitreous phase, and no other defects, in terms of unsaturated bonds or different bonding arrangements, were found.<sup>9a,15</sup> Despite this, both the amorphous and crystalline areas sometimes showed local variations of corrugation amplitude (typically,  $< 0.2$  Å), which can be associated with variations of the local density of states (probed by STM), e.g., by formation of strained Si–O–Si siloxanes. Those structures, however, which are parallel to the film surface, still cannot account for the overwhelming preponderance of only one type of OD species in the isotopic experiments, provided hydroxylation goes through route 1. Alternatively, the reaction could proceed via water-induced breaking of the Si–O–Si linkage between the two layers (see the structure in the inset of Figure 1a) due to vertical distortion of the upper Si out of the surface plane upon dissociative binding of  $^{16}\text{OD}$ . However, the vertical Si–O–Si linkage, as judged by IRAS,<sup>9a</sup> is the least suffering from lateral film disordering and, therefore, more stable than the surface Si–O–Si species. Furthermore, hydroxylation occurs at temperatures as low as 200 K, thus implying that the reaction has almost no activation barrier, which is hardly possible on the vertical Si–O–Si linkages, albeit with a high density of water molecules provided by the ice film. In addition, the fate of the second (“invisible”) D atom (ion) remains unclear.

An alternative type of “defect” that we might consider is step edges, which are commonly thought to expose low-coordinated surface atoms and might, thereby, act as active sites for water adsorption. These sites can be present either on a step between two silica terraces, which basically follow the topography of the underlying metal support, or along the border of “holes”, which are also present in the films. Such step edges, in the absence of any reconstruction, must expose very reactive dangling Si–O bonds, which can then be stabilized by hydroxyls in the same manner as cleaved quartz surfaces.<sup>1d,f,h</sup> The high reactivity of such sites could provide an explanation for the frequent observations of small amounts of hydroxyls on the “as-prepared” films, which presumably form through reaction with residual gases in

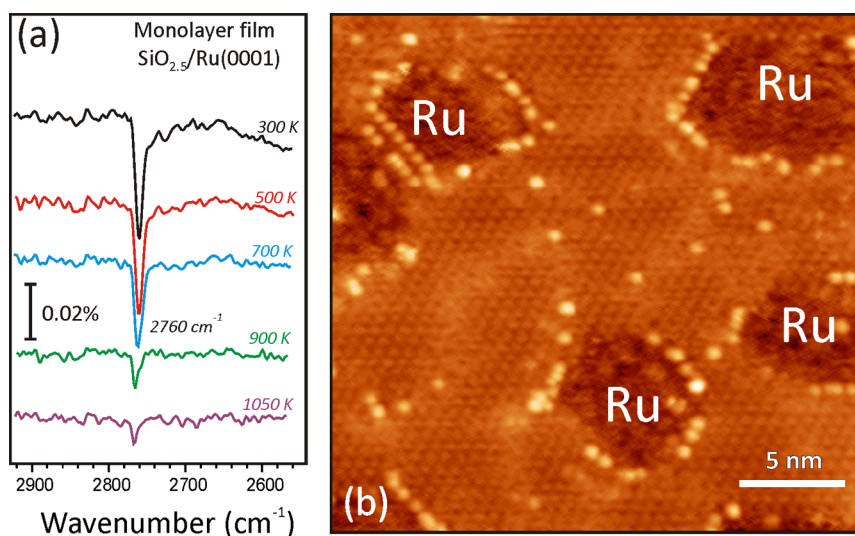


**Figure 4.**  $\nu(\text{OD})$  region of IRA spectra (a) and a room-temperature STM image (b) of a hydroxylated monolayer  $\text{SiO}_{2.5}$  film on  $\text{Ru}(0001)$ . The spectra were measured after  $\text{D}_2\text{O}$  adsorption at 100 K and heating to the indicated temperature. The spectra are offset for clarity. The sample, imaged in (b), intentionally contained many substrate exposing “holes” to demonstrate a decoration of step edges by hydroxo species.

the vacuum background (see below). Unfortunately, direct visualization of surface silanol groups with STM was unsuccessful on the bilayer films, but it was possible on monolayer films.

Figure 4b shows an STM image of a monolayer silica film, which was intentionally created with an abundance of Ru-exposing holes and then hydroxylated in a manner consistent with that already discussed for the bilayer films. The atomically sized protrusions (about 1–2 Å in height), which decorate the holes, appear only upon hydroxylation and are accompanied by the appearance of the band at  $2760\text{ cm}^{-1}$  in IRAS, as shown in Figure 4a. On the basis of this correlation, we have assigned the protrusions to surface hydroxyls. The shortest distance between these protrusions is about 5 Å, i.e., the length of the unit cell in the silica film, indicating that these species are isolated in nature, in agreement with the IRAS results. The preferential binding along the perimeter of the holes suggests that step edges likely provide the majority of the active sites for water dissociation and binding, while the TPD results indicate either a limitation to diffusion confined within those regions or, at a minimum, a lower activation barrier for desorption from them. Noteworthy, the  $\nu(\text{OH})$  band for monolayer films ( $2760\text{ cm}^{-1}$ ) is slightly (by  $5\text{ cm}^{-1}$ ) red-shifted with respect to that for bilayer films, indicating some effect from the chemical bonds between the silica and the metal support.

**3.2. CO and  $\text{NH}_3$  Adsorption on Hydroxylated Silica Films.** The acidity of hydroxyl species on oxides is commonly studied using adsorption of weak and strong bases, such as CO and  $\text{NH}_3$ , respectively. When CO forms an  $\text{OH}\cdots\text{CO}$  adduct, spectral shifts can be noted for both O–H and C–O stretching vibrations, and the magnitude of this shift is a measure of the proton acidity.<sup>16</sup> Strong bases may even abstract a proton.

The hydroxylated films for the CO and  $\text{NH}_3$  adsorption experiments were prepared by water adsorption at 100 K and heating to 300 K in UHV. Continuous exposure of hydroxylated silica films to  $\sim 10^{-5}$  mbar CO at 300 K causes no change in the position or integral intensity of the  $\nu(\text{OD})$  band at  $2765\text{ cm}^{-1}$  (Figure 5). Additionally, the only change we note is the appearance of a signal at  $\sim 2050\text{ cm}^{-1}$  that quickly saturates with increasing CO exposure. This band can be

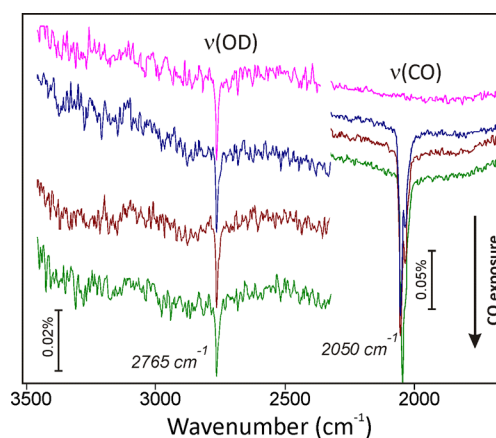


**Figure 5.**  $\nu(\text{OD})$  and  $\nu(\text{CO})$  regions in the IRA spectra of bilayer silica films before (top spectrum) and during CO exposure at 300 K. The spectra are offset for clarity.

straightforwardly assigned to atop CO species binding over Ru in areas exposed by “holes” or large pores within amorphous domains of the silica film.<sup>9a</sup> Therefore, we conclude that CO does not interact with silanols, which differs from results obtained over Al-doped silica films, where highly acidic bridging ( $\text{Si}-\text{OH}-\text{Al}$ ) hydroxyls are produced.<sup>17</sup> For comparison, the “as-prepared” films showed the  $\nu(\text{CO})$  band at  $\sim 2075\text{ cm}^{-1}$ , characteristic for the O-precovered Ru surface in the film holes.<sup>9a</sup> Therefore, it appears that the combination of water adsorption and subsequent desorption acts to remove O atoms directly adsorbed on Ru within the more porous areas of the film.

Since no interaction was observed between hydroxyls and coadsorbed CO, we also probed the surface with  $\text{NH}_3$  to determine if the stronger base might show some reactivity. When dosing at room temperature, only subtle changes could be detected in situ by IRAS. Contrastingly, the TPD spectra shown in Figure 6 do provide evidence of some reactivity following exposure of the prehydroxylated surface to ammonia. At this point it is instructive to recall that masses 17 and 16 correspond to  $\text{NH}_3^+$  and  $\text{NH}_2^+$  ions of  $\text{NH}_3$  in a mass

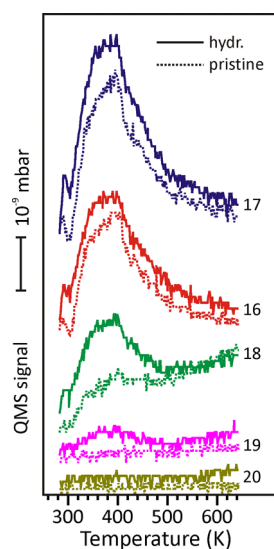


**Figure 6.** TPD signals for indicated masses after adsorption of 25 L of  $\text{NH}_3$  onto pristine (dashed lines) and OD-containing (solid lines) bilayer silica films at 300 K. The spectra are offset for clarity.

spectrometer. The 20 amu is associated with  $\text{D}_2\text{O}$ , which also contributes to the 18 and 16 amu signals as  $\text{DO}^+$  and  $\text{O}^+$ , respectively. In addition, the 18 amu is also the principal signal from  $\text{H}_2\text{O}$ , which in turn contributes to the 17 amu ( $\text{OH}^+$ ) and 16 amu ( $\text{O}^+$ ) signals. Finally, the mass 19 can be assigned to  $\text{HDO}$ , which also has fragments at 18, 17, and 16 amu's, while D-substituted ammonia  $\text{NH}_{3-x}\text{D}_x$  exhibits different masses depending on  $x$ .

The most obvious difference between the TPD spectra from the pristine and hydroxylated surfaces (Figure 6) is observed for the 18 amu signal. Certainly, this feature cannot be associated with  $\text{D}_2\text{O}$  since the 20 amu signal is negligible. In principle,  $\text{H}_2\text{O}$  could be formed as the result of OH recombination following a H–D exchange reaction between OD and  $\text{NH}_3$ , but the desorption temperature ( $\sim 400$  K) is clearly too low for this; we, therefore, propose that the creation and desorption of  $\text{NH}_2\text{D}$  provides a more plausible explanation of this signal's origin. In such exchange reactions, one should also consider formation of  $\text{NHD}_2$  (19 amu) and  $\text{ND}_3$  (20 amu), which turned out to be almost negligible under the conditions of this experiment.

To increase the sticking probability, we have also studied  $\text{NH}_3$  adsorption at low temperatures. Again, TPD measurements show evidence of reaction between the  $\text{NH}_3$  and coadsorbed hydroxyls, which manifests itself as a second desorption feature at 150 K (Figure 7a) and is not observed for ammonia TPD from pristine samples (Figure 7b). The mass-dependent breakdown of the signal in this feature shows significant intensity for every channel associated with  $\text{ND}_x\text{H}_y$  ion detection, but qualitatively, the entire distribution appears to be shifted by 1 amu to larger values relative to that from the low-temperature feature (Figure 7c).

Assuming that the signal at  $\sim 115$  K results from molecular desorption of contaminant-free  $\text{NH}_3$ , we can deduce that the relative abundance of masses 18, 19, and 20 in this feature arise through H–D exchange during wall reactions within the mass spectrometer. Using methodologies outlined in the Supporting Information, in conjunction with the  $\text{NH}_3$  cracking pattern, we can then use the relative abundances of those masses to estimate the likelihood of exchanging 1, 2, or 3 hydrogen(s) for

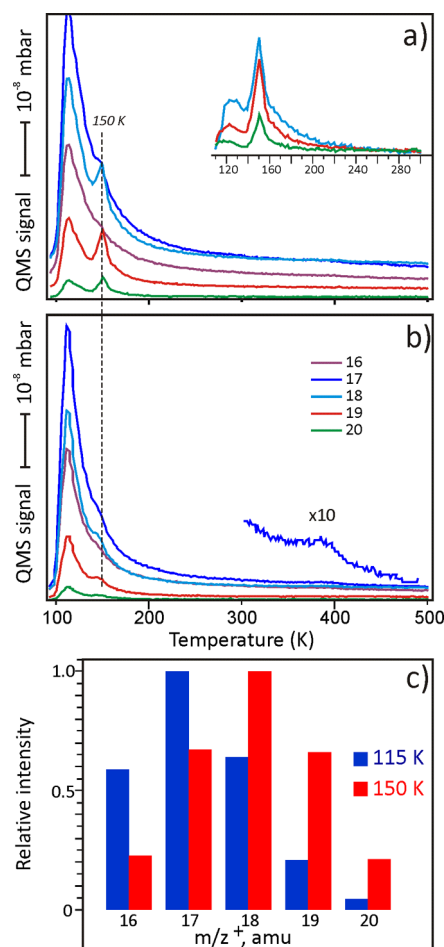


**Figure 7.** TPD signals of 25 L of  $\text{NH}_3$  adsorbed over hydroxylated (a) and pristine (b) bilayer  $\text{SiO}_2/\text{Ru}(0001)$  samples ( $T_{\text{ads}} = 100$  K) are shown for several masses of interest. (c) The relative abundance of the various masses probed in (a) are shown for the two desorption features, i.e., at 115 and 150 K.

deuterium via wall reaction and, from that, predict the relative abundances of  $m/z^+ = 16\text{--}20$  that would be expected for the case when 1 H–D exchange takes place to form  $\text{NDH}_2$  on the surface prior to desorption into the mass spectrometer. On the basis of the good agreement of such a distribution with our experimental data (see Figure S3, Supporting Information), we conclude that the signal at 150 K results predominantly from desorption of  $\text{NDH}_2$  produced in this manner. Interestingly, a small desorption feature is also detected at  $\sim 400$  K (see Figure 7b), which is almost the same temperature at which ammonia desorption was noted after adsorption at 300 K (Figure 6).

To better understand the surface chemistry driving this reaction, we have also carried out a complementary low-temperature IRAS study. Figure 8 shows a series of spectra taken from hydroxylated silica after  $\text{NH}_3$  adsorption at  $\sim 90$  K and subsequent flashes to the indicated temperatures. To highlight spectral changes, the spectra have been divided by a reference spectrum, which was taken prior to ammonia adsorption. Molecularly adsorbed ammonia manifests itself as a peak at  $3406\text{ cm}^{-1}$  and a broad band at  $3000\text{--}3500\text{ cm}^{-1}$ , which is assigned to the asymmetric and symmetric N–H stretching vibrations in  $\text{NH}_3$  (top spectrum in Figure 8).<sup>18</sup> Additional bands were also observed in the region of N–H

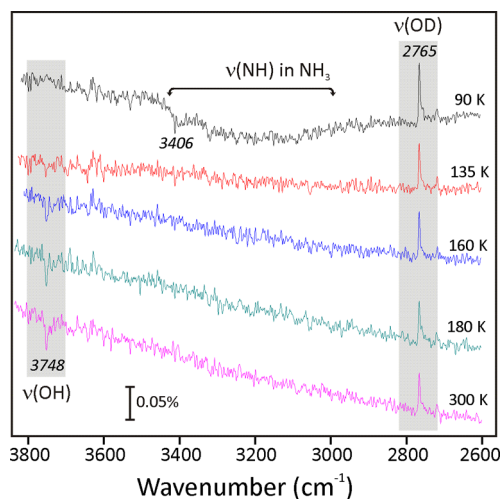


**Figure 8.** IRA spectra of an OD-containing bilayer silica film after adsorption of  $\text{NH}_3$  at 90 K and heating to the indicated temperature. The spectra are referenced to a spectrum taken before ammonia adsorption and are offset with the  $\nu(\text{OD})$  and  $\nu(\text{OH})$  bands highlighted for clarity.

deformation modes at  $1635\text{--}1600\text{ cm}^{-1}$  (not shown). (Note that the relative intensity may be affected by the metal selection rules.)<sup>13</sup>

Upon arrival of the ammonia features at 90 K, we also note the concomitant loss of the  $\nu(\text{OD})$  band, which results in a positive signal at  $2765\text{ cm}^{-1}$ . After heating to 135 K, which is below the second desorption maximum at 150 K (see Figure 7), the  $\nu(\text{NH})$  bands vanish since the more weakly bound ammonia desorbs intact at these temperatures. After heating to 160 K, and further to 300 K, the intensity of the positive  $\nu(\text{OD})$  signal at  $2765\text{ cm}^{-1}$  diminishes only slightly, indicating that the majority of the OD species are consumed by reaction with ammonia. Meanwhile, a  $\nu(\text{OH})$  band at  $3748\text{ cm}^{-1}$  becomes apparent by 160 K and saturates by 180 K, which seems to validate our TPD analysis (i.e., that H–D exchange occurs between OD and  $\text{NH}_3$  at low temperatures to form D-substituted ammonia, which then desorbs, leaving behind OH species).

The absence of  $\text{NH}_3$  in the 150 K desorption feature, and the absence of this feature altogether from pristine films, can be explained by: (i) ammonia is more strongly bound to surface hydroxyls, and (ii) the exchange reaction goes with a high conversion, such that no hydroxyl-bound  $\text{NH}_3$  survives, and almost all ODs transform into OHs, as Figure 8 suggests. As such, the peak desorption temperature (149 K) can be used to estimate an upper limit to the activation barrier for the H–D reaction, which is calculated to be  $\sim 37\text{ kJ/mol}$  using a Redhead formalism<sup>19</sup> with a prefactor  $\nu_0 = 10^{13}\text{ s}^{-1}$  corresponding to OH (OD) stretching vibrations.

To examine whether the exact nature of the silanol groups (isolated vs H-bonded) is especially important in facilitating the H–D reaction with ammonia, we measured the production of  $\text{NH}_2\text{D}$  (at 140–180 K) as a function of the annealing temperature of OD-containing films before  $\text{NH}_3$  adsorption (Figure 9). In this case, the measurements were carried out sequentially over the same film, which was regenerated via high-temperature oxidation and subsequent  $\text{D}_2\text{O}$  hydroxylation before each heating step (300, 600, and 900 K). The respective IRA spectra of the samples are depicted in the inset in Figure 9. As mentioned earlier, high-temperature annealing results in the

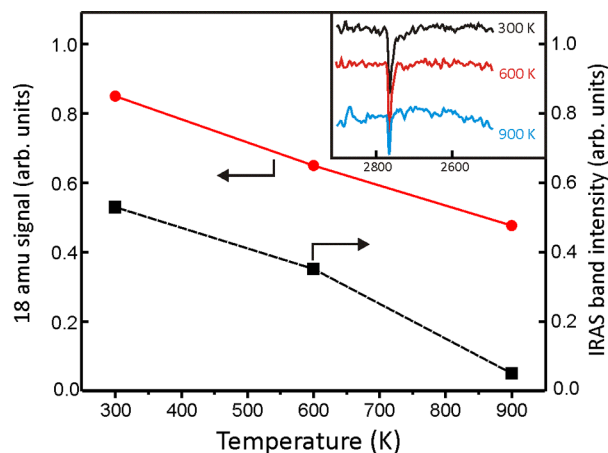


**Figure 9.** Integral intensities of the 18 amu signal at 140–180 K (see Figure 7) and of the IRAS peak at  $2765\text{ cm}^{-1}$  (see inset) as a function of the annealing temperature of an OD-containing bilayer silica film.

formation of isolated silanols, whereas annealing to 300 K seems to result in H-bonded species as well. As we appear to note a linear dependence of the H–D exchange reaction on the total number of OD groups, with no significant deviation when H-bonded species are present, we conclude that each hydroxyl interacts independently with the coadsorbed ammonia during the H–D exchange reaction.

Finally, we studied ammonia adsorption over  $^{18}\text{O}$ -prepared silica, which also revealed some interesting results. The top spectrum in Figure 10 shows a spectrum from a  $\text{Si}^{18}\text{O}_2$  film that

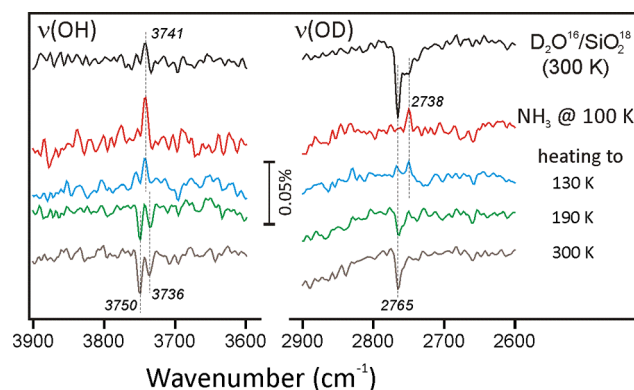


**Figure 10.** IRA spectrum of a  $\text{Si}^{18}\text{O}_2$  film exposed to  $\text{D}_2^{16}\text{O}$  at 100 K and heated to 300 K (top), which was then exposed to  $\text{NH}_3$  at 100 K and heated to the indicated temperatures. All spectra are referenced to a spectrum from the “as-prepared” film taken before  $\text{D}_2^{16}\text{O}$  adsorption and are offset for clarity.

was exposed to  $\text{D}_2^{16}\text{O}$  at 100 K and then heated to 300 K. Here, again, the data are plotted relative to a reference spectrum, which, in this case, was taken from the “as-prepared” film before hydroxylation in this case. As with the unlabeled  $\text{SiO}_2$  (see Figure 2), the OD region is again dominated by a peak at  $2765\text{ cm}^{-1}$  (i.e.,  $^{16}\text{OD}$ ) following hydroxylation of the  $^{18}\text{O}$ -substituted film. Close inspection of the  $\nu(\text{OH})$  region, however, reveals a tiny positive signal at  $3741\text{ cm}^{-1}$ , which is assigned to traces of  $^{18}\text{OH}$  in the reference  $\text{Si}^{18}\text{O}_2$  sample. Although these  $^{18}\text{OH}$  species may undergo H–D exchange upon hydroxylation with  $\text{D}_2^{16}\text{O}$ , the additional contribution to  $^{18}\text{OD}$ -related IRA signals is obviously small.

As expected,  $\text{NH}_3$  adsorption at 100 K completely suppresses the  $\nu(\text{OD})$  band (second spectrum from the top in Figure 10). However, at the same time, a new positive signal is detected at  $2738\text{ cm}^{-1}$  for  $^{18}\text{OD}$ , and the positive signal at  $3741\text{ cm}^{-1}$  ( $^{18}\text{OH}$ ) even gains some intensity. This indicates the presence of adventitious  $^{18}\text{OD}$  and  $^{18}\text{OH}$  species in the reference sample, which most likely come from reaction of highly hydrophilic Si–O dangling bonds with residual gases in the vacuum background (i.e.,  $\text{H}_2\text{O}$  and  $\text{D}_2\text{O}$  accumulated over the course of several experiments). Additionally, this result suggests that low-temperature (100 K)  $\text{NH}_3$  adsorption effectively titrates all hydroxyl species in the sample, irrespective of their origin.

Thermal desorption of ammonia results in the partial recovery of the  $\nu(^{16}\text{OD})$  band at  $2765\text{ cm}^{-1}$  and the appearance of a  $\nu(^{16}\text{OH})$  band at  $3750\text{ cm}^{-1}$ , which is expected for H–D exchange (bottom spectrum in Figure 10). Comparing the top and bottom spectra, that is, before and after reaction with  $\text{NH}_3$ , we see that the intensity of the resultant  $\nu(^{16}\text{OH})$  feature is nearly equal to the attenuation of the  $\nu(^{16}\text{OD})$  band. Interpretation of the  $^{18}\text{O}$ -labeled counterparts is not as straightforward due to the absence of a well-resolved peak corresponding to  $^{18}\text{OD}$  after hydroxylation (top spectrum). Despite this, the fact that the  $\nu(^{18}\text{OH})$  signal at  $3736\text{ cm}^{-1}$  in the bottom spectrum roughly mirrors the positive signal from  $\nu(^{18}\text{OD})$  at  $2738\text{ cm}^{-1}$  in the second spectrum suggests that the majority of the new  $^{18}\text{OH}$ s originated via H–D exchange of  $^{18}\text{OD}$ s that were already present before  $\text{D}_2^{16}\text{O}$  adsorption. As such, the data are consistent with our earlier analysis, which showed minimal evidence of lattice oxygen incorporation into the hydroxyls forming after exposure to water and reveals that the H–D exchange reaction occurs on each OH site, independent of origin. In addition, the observation of two well-resolved peaks in the OH region, for both  $^{18}\text{O}$ - and  $^{16}\text{O}$ -labeled species, casts some additional doubt upon our previously postulated “energy borrowing” and metal selection rule explanations of the IRAS data in Figure 2. Therefore, it seems that hydroxylation proceeds via OH–Si bond formation following exposure to water, which must leave excess H atoms on the surface, the eventual fate of which remains unknown. Of the possible methods of hydrogen removal, recombinative desorption of weakly bound  $\text{H}_2$  and/or capture by the metal support seem most plausible. It is noteworthy that the hydroxylated monolayer films showed the same behavior with respect to the H–D reaction with ammonia (data not shown), only with desorption peaks at a slightly higher temperature ( $\sim 160\text{ K}$ ) compared to bilayer films ( $\sim 150\text{ K}$ ).

#### 4. CONCLUSIONS

Using a combination of TPD, IRAS, and STM, we have studied both the mechanism for formation and the resultant fundamental properties of hydroxyl species present over Ru(0001)-supported ultrathin silica films following exposure to water at different temperatures. From this, we find that hydroxylation most likely occurs almost exclusively at Si–O defect-rich step edges via barrierless reaction at low temperature. Furthermore, the reaction mechanism appears to proceed via dissociation of O–H bonds within water molecules upon formation of intermediate  $\text{H}_2\text{O}\cdots\text{Si}$  complexes, which then create silanol groups, and a free hydrogen atom. Unlike studies over conventional silica materials, the cleaved hydrogens do not appear to bind stably to our films and instead leave the surface via some combination of recombinative desorption and diffusion into the metal support. The silanol bond strengths

seem to be roughly consistent with those in bulk silicates, but recombinative desorption appears to occur almost exclusively from the sites where dissociation first occurred, such that very little lattice oxygen becomes incorporated into the desorbing water molecules.

Using CO, water, and  $\text{NH}_3$  to probe the chemical properties of the silanols, we found no evidence of acidic species but noted a close similarity between the reactions of surface hydroxyls with ammonia and water, where OH species can be replaced by OD and vice versa. The latter finding strongly suggests that the reaction between hydroxyls and ammonia likely proceeds via the same mechanism as that between OD(OH) and  $\text{H}_2\text{O}(\text{D}_2\text{O})$ . In the case of ammonia,  $[\text{NH}_3]\cdots[\text{OD}]$  complexes appeared to interact slightly more strongly than the ammonia present over the remainder of the silica. As the ammonia desorbing from such complexes was almost exclusively in the form of  $\text{NDH}_2$ , we have used the ammonia desorption energy of  $\sim 37\text{ kJ/mol}$  as an upper limit approximation of the H–D exchange activation barrier.

#### ■ ASSOCIATED CONTENT

##### Supporting Information

Additional experimental details and figures. This material is available free of charge via the Internet at <http://pubs.acs.org>.

#### ■ AUTHOR INFORMATION

##### Corresponding Author

\*E-mail: [shaikhutdinov@fhi-berlin.mpg.de](mailto:shaikhutdinov@fhi-berlin.mpg.de). Phone: +49 30 84134114.

##### Notes

The authors declare no competing financial interest.

#### ■ ACKNOWLEDGMENTS

This work was supported by the Fonds der Chemischen Industrie and Deutsche Forschungsgemeinschaft through CoE “UniCat”. MS acknowledges funding from the European Research Council (FP7), ERC Grant agreement No. 280070, STRUBOLI. WK and JAB thank the Alexander von Humboldt Foundation for fellowships. XY and EE acknowledge the International Max-Planck Research School “Complex surfaces in materials science”.

#### ■ REFERENCES

- (1) (a) Zhuravlev, L. T. The Surface Chemistry of Amorphous Silica. Zhuravlev Model. *Colloids Surf., A* **2000**, *173*, 1–38. (b) Chuang, I. S.; Maciel, G. E. A Detailed Model of Local Structure and Silanol Hydrogen Bonding of Silica Gel Surfaces. *J. Phys. Chem. B* **1997**, *101*, 3052–3064. (c) Tielens, F.; Gervais, C.; Lambert, J. F. o.; Mauri, F.; Costa, D. Ab Initio Study of the Hydroxylated Surface of Amorphous Silica: A Representative Model. *Chem. Mater.* **2008**, *20*, 3336–3344. (d) Yang, J.; Wang, E. G. Water Adsorption on Hydroxylated  $\alpha$ -quartz (0001) Surfaces: From Monomer to Flat Bilayer. *Phys. Rev. B* **2006**, *73*, 035406. (e) Bunker, B. C.; Haaland, D. M.; Michalske, T. A.; Smith, W. L. Kinetics of Dissociative Chemisorption on Strained Edge-Shared Surface Defects on Dehydroxylated Silica. *Surf. Sci.* **1989**, *222*, 95–118. (f) Murashov, V. V. Reconstruction of Pristine and Hydrolyzed Quartz Surfaces. *J. Phys. Chem. B* **2005**, *109*, 4144–4151. (g) Bordiga, S.; Ugliengo, P.; Damin, A.; Lamberti, C.; Spoto, G.; Zecchina, A.; Spanò, G.; Buzzoni, R.; Dalloro, L.; Rivetti, F. Hydroxyls Nests in Defective Silicalites and Strained Structures Derived upon Dehydroxylation: Vibrational Properties and Theoretical Modelling. *Top. Catal.* **2001**, *15*, 43–52. (h) Goumans, T. P. M.; Wander, A.; Brown, W. A.; Catlow, C. R. A. Structure and Stability of

the (001)  $\alpha$ -Quartz Surface. *Phys. Chem. Chem. Phys.* **2007**, *9*, 2146–2152.

(2) (a) Morrow, B. A.; McFarlan, A. J. Surface Vibrational Modes of Silanol Groups on Silica. *J. Phys. Chem.* **1992**, *96*, 1395–1400.

(b) Morrow, B. A.; McFarlan, A. J. Infrared and Gravimetric Study of an Aerosil and a Precipitated Silica Using Chemical and Hydrogen/Deuterium Exchange Probes. *Langmuir* **1991**, *7*, 1695–1701.

(c) Hoffmann, P.; Knözinger, E. Novel Aspects of Mid and Far IR Fourier Spectroscopy Applied to Surface and Adsorption Studies on SiO<sub>2</sub>. *Surf. Sci.* **1987**, *188*, 181–198.

(3) Rignanese, G. M.; Charlier, J. C.; Gonze, X. First-Principles Molecular-Dynamics Investigation of the Hydration Mechanisms of the (0001)  $\alpha$ -Quartz Surface. *Phys. Chem. Chem. Phys.* **2004**, *6*, 1920–1925.

(4) Chuang, I. S.; Kinney, D. R.; Maciel, G. E. Interior Hydroxyls of the Silica Gel System as Studied by Silicon-29 CP-MAS NMR spectroscopy. *J. Am. Chem. Soc.* **1993**, *115*, 8695–8705.

(5) Shaikhutdinov, S.; Freund, H.-J. Ultrathin Silica Films on Metals: The Long and Winding Road to Understanding the Atomic Structure. *Adv. Mater.* **2013**, *25*, 49–67.

(6) Weissenrieder, J.; Kaya, S.; Lu, J. L.; Gao, H. J.; Shaikhutdinov, S.; Freund, H. J.; Sierka, M.; Todorova, T. K.; Sauer, J. Atomic Structure of a Thin Silica Film on a Mo(112) Substrate: A Two-Dimensional Network of SiO<sub>4</sub> Tetrahedra. *Phys. Rev. Lett.* **2005**, *95*, 076103.

(7) Löffler, D.; Uhlrich, J. J.; Baron, M.; Yang, B.; Yu, X.; Lichtenstein, L.; Heinke, L.; Buechner, C.; Heyde, M.; Shaikhutdinov, S.; Freund, H. J.; Włodarczyk, R.; Sierka, M.; Sauer, J. Growth and Structure of Crystalline Silica Sheet on Ru(0001). *Phys. Rev. Lett.* **2010**, *105*, 146104.

(8) (a) Wendt, S.; Frerichs, M.; Wei, T.; Chen, M. S.; Kempter, V.; Goodman, D. W. The Interaction of Water With Silica Thin Films Grown on Mo(112). *Surf. Sci.* **2004**, *565*, 107–120. (b) Kaya, S.; Weissenrieder, J.; Stacchiola, D.; Shaikhutdinov, S.; Freund, H. J. Formation of an Ordered Ice Layer on a Thin Silica Film. *J. Phys. Chem. C* **2007**, *111*, 759–764.

(9) (a) Yang, B.; Kaden, W. E.; Yu, X.; Boscoboinik, J. A.; Martynova, Y.; Lichtenstein, L.; Heyde, M.; Sterrer, M.; Włodarczyk, R.; Sierka, M.; et al. Thin Silica Films on Ru(0001): Monolayer, Bilayer and Three-Dimensional Networks of [SiO<sub>4</sub>] tetrahedra. *Phys. Chem. Chem. Phys.* **2012**, *14*, 11344–11351. (b) Lichtenstein, L.; Büchner, C.; Yang, B.; Shaikhutdinov, S.; Heyde, M.; Sierka, M.; Włodarczyk, R.; Sauer, J.; Freund, H.-J. The Atomic Structure of a Metal-Supported Vitreous Thin Silica Film. *Angew. Chem., Int. Ed.* **2012**, *51*, 404–407.

(10) Morrow, B. A.; Cody, I. A.; Lee, L. S. M. Infrared Studies of Reactions on Oxide Surfaces. 7. Mechanism of the Adsorption of Water and Ammonia on Dehydroxylated Silica. *J. Phys. Chem.* **1976**, *80*, 2761–2767.

(11) (a) Wovchko, E. A.; Camp, J. C.; Glass, J. A.; Yates, J. T. Active Sites on SiO<sub>2</sub>: Role in CH<sub>3</sub>OH Decomposition. *Langmuir* **1995**, *11*, 2592–2599. (b) Morrow, B. A.; Cody, I. A. Infrared Studies of Reactions on Oxide Surfaces. 5. Lewis Acid Sites on Dehydroxylated Silica. *J. Phys. Chem.* **1976**, *80*, 1995–1998.

(12) Chiang, C. M.; Zegarski, B. R.; Dubois, L. H. First Observation of Strained Siloxane Bonds on Silicon Oxide Thin Films. *J. Phys. Chem.* **1993**, *97*, 6948–6950.

(13) Hoffmann, F. M. Infrared Reflection-Absorption Spectroscopy of Adsorbed Molecules. *Surf. Sci. Rep.* **1983**, *3*, 107–192.

(14) Persson, B. N. J.; Ryberg, R. Vibrational Interaction Between Molecules Adsorbed on a Metal Surface: The Dipole–Dipole Interaction. *Phys. Rev. B* **1981**, *24*, 6954–6970.

(15) (a) Lichtenstein, L.; Heyde, M.; Freund, H.-J. Crystalline–Vitreous Interface in Two Dimensional Silica. *Phys. Rev. Lett.* **2012**, *109*, 106101. (b) Heyde, M.; Shaikhutdinov, S.; Freund, H. J. Two-Dimensional Silica: Crystalline and Vitreous. *Chem. Phys. Lett.* **2012**, *550*, 1–7.

(16) Zecchina, A.; Lamberti, C.; Bordiga, S. Surface Acidity and Basicity: General Concepts. *Catal. Today* **1998**, *41*, 169–177.

(17) Boscoboinik, J. A.; Yu, X.; Yang, B.; Fischer, F. D.; Włodarczyk, R.; Sierka, M.; Shaikhutdinov, S.; Sauer, J.; Freund, H.-J. Modeling

Zeolites with Metal-Supported Two-Dimensional Aluminosilicate Films. *Angew. Chem., Int. Ed.* **2012**, *51*, 6005–6008.

(18) Morimoto, T.; Yanai, H.; Nagao, M. Infrared Spectra of Ammonia Adsorbed on Zinc Oxide. *J. Phys. Chem.* **1976**, *80*, 471–475.

(19) Redhead, P. A. Thermal Desorption of Gases. *Vacuum* **1962**, *12*, 203–211.